Combined Tevatron Upper Limit on $gg \to H \to W^+W^-$ and Constraints on Fourth-Generation Fermion Models

(Dated: March 12, 2010)

We combine results from CDF and D0 searches for a standard model Higgs boson (H) in the process $gg \to H \to W^+W^-$ in $p\bar{p}$ collisions at the Fermilab Tevatron at $\sqrt{s} = 1.96$ TeV. With 4.8 fb^{-1} of integrated luminosity analyzed at CDF and 5.4 fb^{-1} at D0, the 95% C.L. upper limit on $\sigma(gg \to H) \times Br(H \to W^+W^-)$ is 1.77 pb at $m_H = 120$ GeV, 0.41 pb at $m_H = 165$ GeV, and 1.05 pb at $m_H = 260$ GeV. Assuming the existence of a sequential fourth generation of fermions with very large masses, we exclude a standard-model-like Higgs boson with a mass between 130 and 210 GeV.

PACS numbers: 13.85.Rm, 14.80.Bn, 14.65.Jk

Exploring the mechanism for breaking of the $SU(2) \times U(1)$ electroweak gauge symmetry is a high priority in particle physics. Not only are this symmetry and its breaking [1] necessary components for the consistency of the standard model (SM) [2], but measurable properties of the breaking mechanism can potentially be sensitive to new phenomena. Making these measurements, or setting limits in the absence of observation, can be used to constrain broad classes of extensions to the SM.

A natural extension to the SM that can be tested with Higgs boson searches at the Tevatron is the addition of a fourth generation of fermions with masses much larger than those of the first three generations [3]. Precision measurements of the Z boson decay width [4] exclude models in which the fourth generation neutrino mass eigenstate has a mass less than 45 GeV. If the masses are very large, however, a fourth generation of fermions is not yet excluded and is consistent will all available precision electroweak measurements [6]. One consequence of the extra fermions is that the ggH coupling is enhanced by a factor of roughly ~ 3 relative to the SM coupling [5]. The reason for this is that the lowest order ggH coupling arises from a quark loop, and the top quark contribution dominates due to its large coupling with the Higgs boson. In the limit $2m_{f4} \gg m_H$ where m_{f4} is the mass of any fourth-generation quark, the Higgs boson coupling cancels the mass dependence for each of the three propagators in the loop, and the contribution to the ggH becomes asymptotically independent of the masses of the two fourth-generation quarks. Each fourth-generation quark then contributes as much as the top quark, and the ggH coupling is enhanced by a factor $K_e \approx 3$ for low Higgs masses.

The production cross section is enhanced by a factor of $\sim K_e^2$, which ranges from 9 for m_H near the low end of our search range ($m_H = 110$ GeV) to about 7.5 near the upper end of the search range ($m_H = 260$ GeV), assuming asymptotically large masses for the fourth-generation quarks. The reason for the smaller enhancement factor at higher m_H is that the top quark contribution grows larger as m_H nears $2m_t$ and the interaction approaches resonance. For lower-mass fourth-generation quarks, enhancements due to resonances in the loop increase the value of K_e. The partial decay width for $H \to gg$ is enhanced by the same factor as the production cross section. Because the decay $H \to gg$ is mediated through a loop diagram and therefore suppressed by α_s^2, the $H \to W^+W^-$ decay still dominates for Higgs boson masses $m_H > 135$ GeV.

We consider two fourth-generation scenarios. In the first, called the "infinite-mass" scenario, we set the masses of all fourth-generation fermions to 10 TeV. In the second, called the "low-mass" scenario, we set the masses close to their experimental limits [7]. In particular, we set $m_{\ell 4} = 100$ GeV, $m_{\nu 4} = 80$ GeV, $m_{u4} = 256$ GeV, and $m_{d4} = 128$ GeV. In the infinite-mass scenario, the fourth-generation fermions only play a role in the Higgs boson production via loops, while in the low-mass scenario, Higgs boson decays to $\ell_4^+\ell_4^-$, $\nu_4\bar{\nu}_4$, and $d_4\bar{d}_4$ become possible for Higgs boson masses above the respective thresholds. As the decays to the fourth-generation fermions open up, the branching ratio $Br(H \to W^+W^-)$ decreases.

Previously, the CDF and D0 collaborations have published searches for the process $gg \to H \to W^+W^-$ [8, 9]. The D0 search includes a fourth-generation interpretation. Recently the CDF and D0 collaborations have sought the SM Higgs boson in the decay $H \to W^+W^-$ using all SM production processes, $gg \to H$, $qq \to WH$, $qq \to ZH$, and VBF [10–12]. Because only the ggH coupling is enhanced and the WWH and ZZH couplings are not, and because the signal acceptances and the backgrounds in the different analyses differ for the several production modes, the results of these searches cannot be used directly to constrain fourth-generation models as they rely on the SM to predict the ratios of the production rates. Using published analyses with 4.8 fb^{-1} from CDF [10] and 5.4 fb^{-1} from D0 [11], we present new limits on $\sigma(gg \to H) \times Br(H \to W^+W^-)$ in which only the $gg \to H$ production mechanism is considered as signal. These limits are compared to models for Higgs production in which the ggH coupling is enhanced by

the presence of a fourth generation of fermions. In this comparison, the decay branching ratios of the Higgs boson are also modified to reflect changes due to the fourth generation relative to the SM prediction. While decays of the heavy leptons and quarks may in fact include W bosons in the final state, we do not include these as potential signals. The branching ratios for $H \to W^+W^-$ are calculated using HDECAY [13] modified to include fourth-generation fermions [6].

The event selections are similar for the CDF and D0 analyses with details provided in Ref. [10, 11]. Both collaborations select events with large missing transverse energy ($\not\!\!E_T$) and two oppositely-charged, isolated leptons, targeting the $H \to W^+W^-$ signal in which both W bosons decay leptonically. The D0 analysis classifies events in three channels defined by the charged leptons (e or μ), e^+e^-, $e^\pm\mu^\mp$, and $\mu^+\mu^-$. The CDF analysis separates opposite-sign candidate events into five non-overlapping channels. Events are classified by their jet multiplicity (0, 1 or ≥ 2), and the 0 and 1 jet channels are further divided according to whether both leptons are in the central part of the detector or whether one lepton is forward. Two changes have been made in the D0 event selection from the analysis presented in Ref. [11]. The requirement on the dilepton ϕ-opening angle ($\Delta\phi(\ell,\ell)$) has been removed for $e^\pm\mu^\mp$ candidate events and relaxed to $\Delta\phi(\ell,\ell) < 2.5$ radians for e^+e^- and $\mu^+\mu^-$ candidate events in order to enhance the acceptance for large $m_H > 200$ GeV. A requirement on the ϕ-opening angle between the highest-p_T muon and the missing transverse energy, $\Delta\phi(\mu, \not\!\!E_T) > 0.5$, has been included to remove additional background in a signal-free region.

The presence of neutrinos in the final state prevents full reconstruction of the Higgs boson mass and thus other variables are used for separating signal from background. For example when considering $m_H \approx 160$ GeV, the angle $\Delta\phi(\ell,\ell)$ in signal events is smaller on average than in background events, the missing transverse energy is larger, and the total transverse energy of the jets is lower. In these analyses, the final discriminants are neural-network outputs based on several kinematic variables [10, 11]. For CDF, the list of network inputs includes likelihoods constructed from matrix-element probabilities.

The details of the signal and background estimations and the systematic uncertainties are provided in Ref. [10–12]. With these predictions, we set limits on $\sigma(gg \to H) \times Br(H \to W^+W^-)$ as a function of m_H, which do not require a prediction for the production rate. We use the same two statistical methods employed in Ref. [12], namely CL_s and Bayesian techniques, in order to study the consistency of the handling of the experimental results, and to verify that the limits do not depend on the details of the statistical method. Each method is applied at each test mass to calculate an observed upper limit on $\sigma(gg \to H) \times Br(H \to W^+W^-)$, and pseudo-experiments drawn from systematically-varied background-only predictions are used to compute the limits we expect to obtain in the absence of a signal. We present both the Bayesian and CL_s observed and expected limits in this paper. Correlated systematic uncertainties are treated in the same way as they are in Ref. [12]. The sources of correlated uncertainty between CDF and D0 are the total inelastic $p\bar{p}$ cross section, the SM diboson background production cross sections (WW, WZ and ZZ), and the $t\bar{t}$ and single-top production cross sections. Common central values of these cross sections are used by the two collaborations before performing the combination. Instrumental effects such as trigger efficiencies, lepton identification efficiencies and misidentification rates, and the jet energy scales used by CDF and D0 remain uncorrelated. When setting limits on $\sigma(gg \to H) \times Br(H \to W^+W^-)$, we do not include the theoretical uncertainty on the prediction of $\sigma(gg \to H) \times Br(H \to W^+W^-)$ in the fourth-generation models; the limits do not depend on the specific theory predictions. However, when setting limits on m_H in the context of fourth-generation models, we include the uncertainties on the theoretical predictions.

For the infinite-mass fourth-generation model, the signal rate prediction is given in Ref. [6], which includes Next-to-Next-to-Leading Order QCD effects [14] but not the two-loop electroweak effects, as they do not receive a fourth-generation enhancement. The $gg \to H$ production rate incorporating the fourth-generation enhancement is determined using the following procedure. The light-quark electroweak contribution [15] is subtracted from the SM $gg \to H$ cross section of [15, 16]. The resulting cross section is then purely from strong interactions and can be scaled by the square of the fourth-generation enhancement factor, K_e [6]. According to [15], the square of the light-quark electroweak terms is negligible, and thus the interference term with the strong-interaction processes is the important piece. We therefore scale the light-quark electroweak contribution previously subtracted by one power of the fourth-generation enhancement factor, K_e, and add this back to compute the total production cross section. The modified Higgs branching ratio to W^+W^- is multiplied by this calculation of the cross section to predict the final fourth-generation enhanced $gg \to H \to W^+W^-$ production cross section. The values of the cross section for $gg \to H \to W^+W^-$ are shown for 110 GeV$< m_H <$ 260 GeV in Table I.

Before computing the cross section limits, we investigate the properties of the signal and background predictions in each analysis bin, as well as those of the observed data. Because there are many channels to combine, we represent the data in a compact form by sorting the bins of each analysis by their signal-to-background ratio s/b, and collect together the predictions and the observations in bins of similar s/b. The comparison of the observations with the predictions is shown in Fig. 1 for the

$m_H = 200$ GeV search. The theory prediction is taken to be that of the infinite-mass scenario. We also show the integrals of these distributions in Fig. 2, starting the integrals from the high-s/b end and proceeding downwards. The background subtracted data is shown in Fig. 3 along with the ± 1 standard deviation on the background and the predicted signal rate for the infinite-mass scenario with $m_H = 200$ GeV. No significant excess is observed in the data, and the theory predicts a measurable excess over the background.

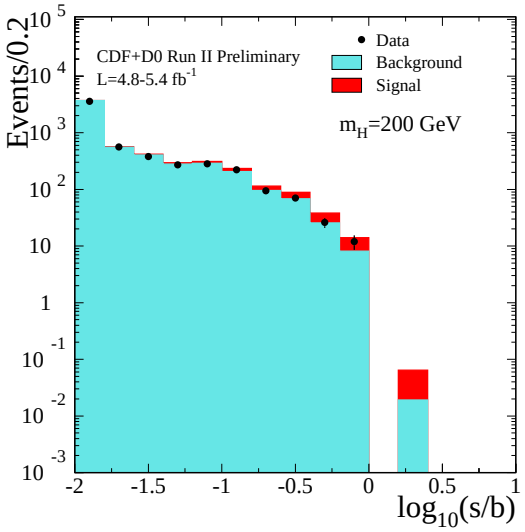

FIG. 1: Signal predictions, background predictions, and observed data, collected in bins sorted by signal divided by background (s/b), for all channels added together, for the search conducted at $m_H = 200$ GeV. The signal expectation, which is shown stacked on top of the background expectation, is normalized to the prediction in the infinite- mass fourth-generation scenario.

The separate limits on $\sigma(gg \to H) \times Br(H \to W^+W^-)$ from CDF and D0 are shown in Figs. 4 and 5 respectively. The combined limits on $\sigma(gg \to H) \times Br(H \to W^+W^-)$ are listed in Table I for both the CL_s and the Bayesian methods, and are shown in Fig. 6 along with the fourth-generation theory prediction for the infinite-mass scenario, as well as for the low-mass scenario.

In order to set limits on m_H in these two scenarios, we perform a second combination, including the uncertainties on the predictions of $\sigma(gg \to H) \times Br(H \to W^+W^-)$ due to scale and PDF uncertainties [15, 16] at each value of m_H tested. The resulting limits are computed relative to the model prediction, and are shown in Fig. 7, for the infinite-mass scenario, which gives the smaller excluded range of m_H. In this scenario, we exclude a SM-like Higgs boson with a mass in the range 130 – 210 GeV. The exclusion region is similar for the low-mass scenario.

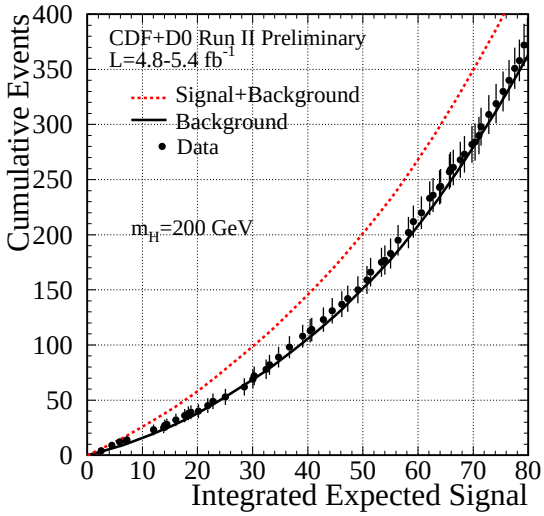

FIG. 2: Integrated signal predictions, background predictions, and observed data, for the search conducted at $m_H = 200$ GeV. The integral is performed so that the highest s/b bins are added first, then collecting lower s/b bins. The signal expectation is normalized to the prediction in the infinite-mass fourth-generation scenario.

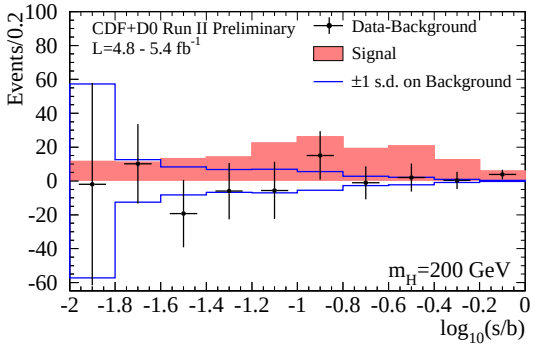

FIG. 3: Background-subtracted data distributions for the discriminant histograms, summed for bins with similar s/b, for the $m_H = 200$ GeV combined search. The background has been fit to the data under the background-only hypothesis, and the uncertainty on the background is the post-fit systematic uncertainty. The uncertainties shown on the background-subtracted data points are the combination of the statistical uncertainty on the post-fit background and the expected statistical uncertainty on the data. The signal, which is normalized to the infinite-mass fourth-generation SM expectation, is shown with a filled histogram.

In summary, we present a combination of CDF and D0 searches for the $gg \to H \to W^+W^-$ process and set

TABLE I: The observed and median expected upper limits on $\sigma(gg \to H) \times Br(H \to W^+W^-)$ in for m_H between 110 GeV and 260 GeV, obtained with the Bayesian and CL_s methods. The predictions of a fourth-generation model with additional fermions for both the infinite-mass and the low-mass scenario are also listed. All limits and predictions are presented in picobarns.

m_H	Bayes		CL_s		4^{th} Gen	4^{th} Gen
[GeV]	Obs.	Exp.	Obs.	Exp.	Inf.-Mass	Low-Mass
110	1.98	1.40	1.92	1.41	0.35	0.38
115	2.35	1.24	2.35	1.22	0.55	0.59
120	1.77	1.08	1.75	1.12	0.80	0.85
125	1.34	0.98	1.33	1.03	1.08	1.15
130	1.26	0.94	1.30	0.98	1.39	1.48
135	1.24	0.89	1.27	0.90	1.70	1.83
140	1.34	0.81	1.33	0.86	2.01	2.16
145	1.00	0.77	0.98	0.81	2.29	2.48
150	0.70	0.66	0.66	0.68	2.55	2.78
155	0.64	0.54	0.63	0.56	2.80	3.08
160	0.51	0.42	0.51	0.41	3.11	3.45
165	0.41	0.37	0.39	0.37	3.07	3.30
170	0.44	0.41	0.43	0.40	2.80	2.93
175	0.40	0.43	0.40	0.45	2.51	2.59
180	0.43	0.47	0.43	0.50	2.21	2.25
185	0.55	0.50	0.54	0.53	1.79	1.83
190	0.50	0.55	0.49	0.56	1.50	1.54
195	0.74	0.57	0.76	0.59	1.32	1.36
200	0.93	0.62	0.92	0.63	1.18	1.22
210	1.02	0.64	1.03	0.66	0.96	0.98
220	1.02	0.63	1.05	0.67	0.80	0.81
230	1.10	0.65	1.11	0.68	0.67	0.68
240	1.12	0.64	1.08	0.69	0.56	0.59
250	1.07	0.61	1.07	0.63	0.48	0.52
260	1.05	0.60	1.06	0.60	0.41	0.46

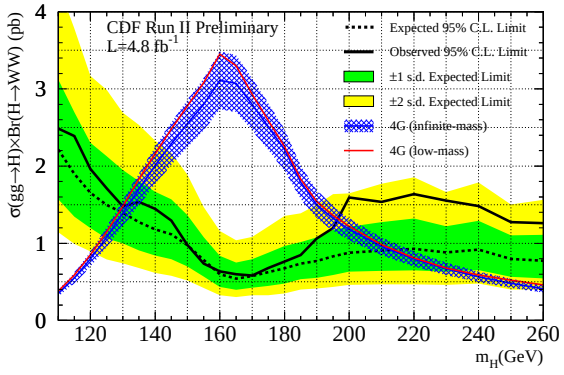

FIG. 4: The CDF observed (solid black line) and median expected (dashed black line) 95% C.L. upper limit on $\sigma(gg \to H) \times Br(H \to W^+W^-)$. The shaded bands indicate the $\pm 1\sigma$ and $\pm 2\sigma$ intervals on the distribution of the limits that are expected if a Higgs boson signal is not present. Also shown is the prediction for a fourth-generation model in the limit that the extra fermions are very heavy. The hatched area indicates the theoretical uncertainty from PDFs and scale uncertainties. The lighter curve shows the low-mass theoretical prediction.

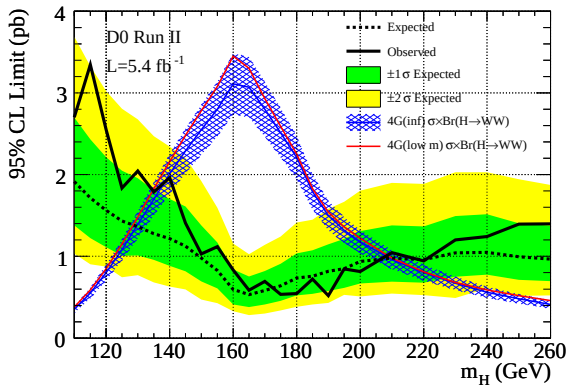

FIG. 5: The D0 observed (solid black line) and median expected (dashed black line) 95% C.L. upper limit on $\sigma(gg \to H) \times Br(H \to W^+W^-)$. The meaning of the $\pm 1\sigma$ and $\pm 2\sigma$ intervals, and of the curves and hatched areas indicating the predictions of fourth-generation models are the same as for Fig. 4.

an upper limit on $\sigma(gg \to H) \times Br(H \to W^+W^-)$ as a function of m_H. We compare these limits with the prediction of the minimal standard model incorporating a sequential fourth generation of infinite-mass fermions and a sequential fourth generation with the mass spec-

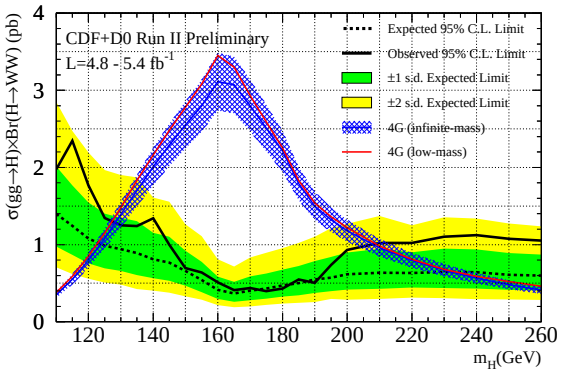

FIG. 6: The combined observed (solid black line) and median expected (dashed black line) 95% C.L. upper limit on $\sigma(gg \to H) \times Br(H \to W^+W^-)$. The meaning of the $\pm 1\sigma$ and $\pm 2\sigma$ intervals, the curves, and the hatched areas indicating the predictions of fourth-generation models are the same as for Fig. 4.

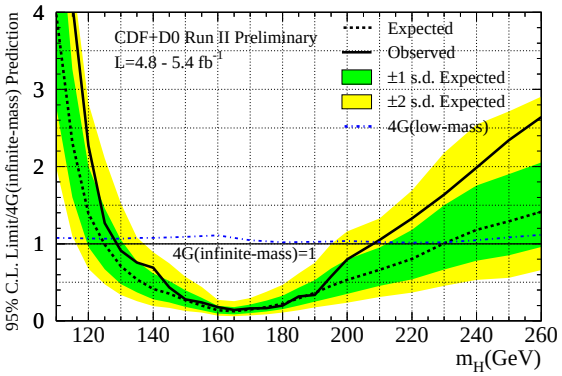

FIG. 7: The CDF+D0 combined test of the "infinite-mass" fourth-generation scenario. The limit is computed using the theoretical uncertainty on the prediction, and the resulting limits and expected limits are shown as ratios to the predicted $\sigma(gg \to H) \times Br(H \to W^+W^-)$. The solid black line shows the ratio of the observed 95% C.L. limit relative to the theoretical prediction, and the dashed black line shows the median expected limit ratio. The shaded bands indicate the $\pm 1\sigma$ and $\pm 2\sigma$ intervals on the distribution of the limits that are expected if a Higgs boson signal is not present. Also shown is the ratio of the low-mass theoretical prediction to that of the infinite-mass scenario (dash-dotted line), which enables extraction of the mass bounds in the low-mass scenario.

trum $m_{\ell 4} = 100$ GeV, $m_{\nu 4} = 80$ GeV, $m_{u4} = 256$ GeV, and $m_{d4} = 128$ GeV. For the infinite-mass scenario we exclude fourth-generation fermions in the mass range 130 GeV$< m_H <$ 210 GeV.

Acknowledgements

[1] P. W. Higgs, Phys. Lett. **12**, 132 (1964); *idem*, Phys. Rev. Lett. **13**, 508 (1964); *idem*, Phys. Rev. **145**, 1156 (1966); F. Englert and R. Brout, Phys. Rev. Lett. **13**, 321 (1964); G. S. Guralnik, C. R. Hagen and T. W. B. Kibble, Phys. Rev. Lett. **13**, 585 (1964).

[2] S. L. Glashow, Nucl. Phys. **22**, 579 (1961); S. Weinberg, Phys. Rev. Lett. **19**, 1264 (1967); A. Salam, *Elementary Particle Theory*, ed. N. Svartholm (Almquist and Wiksells, Stockholm, 1968), 367.

[3] B. Holdom, et al., PMC Phys. A **3**, 4 (2009), and references therein.

[4] The ALEPH, DELPHI, L3, OPAL, SLD Collaborations, the LEP Electroweak Working Group, and the SLD Electroweak and Heavy Flavour Groups, Phys. Rept. **427**, 257 (2006).

[5] E. Arik, O. Cakir, S. A. Cetin and S. Sultansoy, Acta Phys. Polon. B **37**, 2839 (2006).

[6] G. D. Kribs, T. Plehn, M. Spannowsky, and T. M. P. Tait, Phys. Rev. D **76**, 075016 (2007).

[7] C. Amsler *et al.* (Particle Data Group), Phys. Lett. B **667**, 1 (2008).

[8] T. Aaltonen *et al.* [CDF Collaboration], Phys. Rev. Lett. **102**, 021802 (2009).

[9] V. M. Abazov *et al.* [D0 Collaboration], Phys. Rev. Lett. **96**, 011801 (2006).

[10] T. Aaltonen *et al.* [CDF Collaboration], Phys. Rev. Lett. **104**, 061803 (2010).

[11] V. M. Abazov *et al.* [D0 Collaboration], Phys. Rev. Lett. **104**, 061804 (2010).

[12] T. Aaltonen *et al.* [CDF and D0 Collaborations], Phys. Rev. Lett. **104**, 061802 (2010).

[13] A. Djouadi, J. Kalinowski and M. Spira, Comput. Phys. Commun. **108**, 56 (1998).

[14] S. Catani, D. de Florian, M. Grazzini and P. Nason, JHEP **0307**, 028 (2003).

[15] C. Anastasiou, R. Boughezal and F. Petriello, JHEP **0904**, 003 (2009).

[16] D. de Florian and M. Grazzini, Phys. Lett. B **674**, 291 (2009).